


 Cite this: *RSC Adv.*, 2022, **12**, 27625

Improving the efficiency of n-Si/PEDOT:PSS hybrid solar cells by incorporating AuNP-decorated graphene oxide as a nanoadditive for conductive polymers

Nguyen Van Tu,^a Nguyen Ngoc Anh,^a Tran Van Hau,^a Nguyen Van Hao,^c Nguyen Thi Huyen,^a Bui Hung Thang,^a Phan Ngoc Minh,^{ab} Nguyen Van Chuc,^a  Naoki Fukata  and Pham Van Trinh                  <img alt="Email icon" data-bbox="1070

15 nm in diameter were prepared by using the chemical reduction method. The microstructure of GO-AuNP hybrid material was investigated. The effects of the GO-AuNPs hybrid material on the properties of transparent conductive thin film and the hybrid solar cells were also investigated.

2. Experimental

2.1. Preparation of AuNPs decorated GO

The GO-AuNPs hybrid material was prepared by the chemical reduction process. First, 100 ml of a 0.2 mM solution of chloroauric acid ($\text{HAuCl}_4 \cdot 3\text{H}_2\text{O}$, Sigma Aldrich) was introduced to a 500 ml beaker of GO-containing solution (0.1 g l^{-1}) under continuous magnetic stirring. Consequently, a sodium borohydride solution (NaBH_4 , Sigma Aldrich) 0.1 M was slowly added to the solution containing HAuCl_4 and GO under constant stirring. The stirring process was continued for 10 minutes to obtain a homogenous solution. Afterwards, the above solution was filtered and washed with distilled water to obtain GO-AuNP hybrid material. Finally, the hybrid materials were disseminated in deionized water by ultrasonication for 45 minutes and then kept in the dark to reduce oxidation.

2.2. Preparation of PEDOT:PSS/GO-AuNPs thin films

The PEDOT:PSS/GO-AuNPs transparent conductive film was prepared by the following steps: firstly, GO-AuNPs solution with

a concentration 1 mg/1 ml of was put into PEDOT:PSS with a fixed concentrations of 0.5 wt% and then stirred for 6 hours to uniformly disperse GO-AuNPs in the PEDOT:PSS. Secondly, the mixture of PEDOT:PSS/GO-AuNPs is coated on the glass substrate by spin coating method with the condition of 10 seconds (2000 rpm) and followed up 60 seconds (6000 rpm). Finally, the prepared film was annealed at 140°C for 30 minutes with the heating and cooling speed of 2°C per min in a N_2 environment to create thin film structure.

2.3. Preparation of n-Si/PEDOT:PSS/GO-AuNPs hybrid solar cell

The manufacturing process of the solar cells based on n-Si/PEDOT:PSS/GO-AuNPs hybrid structure is illustrated in Fig. 1. The n-Si substrate was firstly treated with a solution of piranha at 130°C for 40 min to remove organic compound on the surface. After that, the treated Si substrate was cleaned in turn with acetone, alcohol and deionized water for several times at room temperature. The n-Si substrate was then processed in a 2% HF solution for two minutes to strip off SiO_2 formed on the surface. Immediately, the PEDOT:PSS/GO-AuNPs compound was coated on the n-Si substrate by using the spin coating at condition of 2000 rpm for 10 s and followed up 6000 rpm for 60 s. The obtained structure was then annealed in N_2 atmosphere at 140°C for 30 min to remove residual water. Finally, the front and back electrodes were fabricated by using the

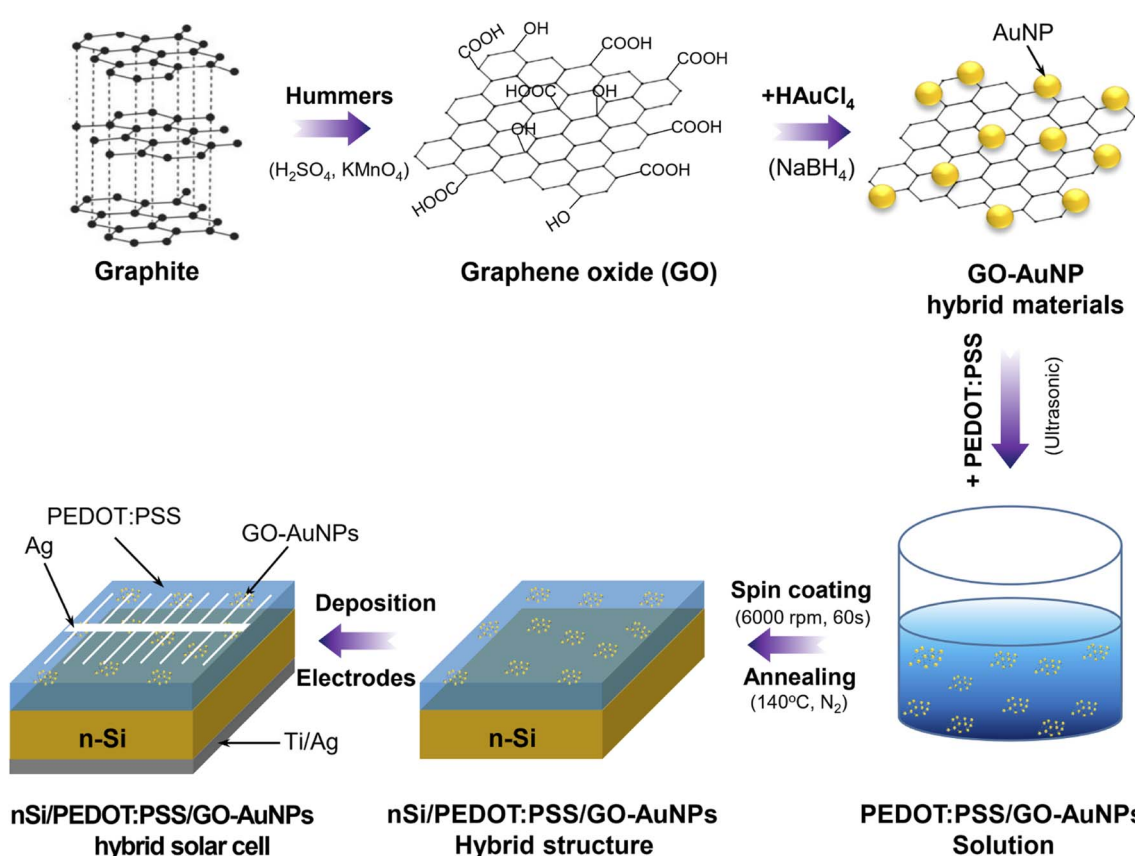


Fig. 1 Schematic view of the preparation process of n-Si/PEDOT:PSS/GO-AuNPs hybrid solar cells.



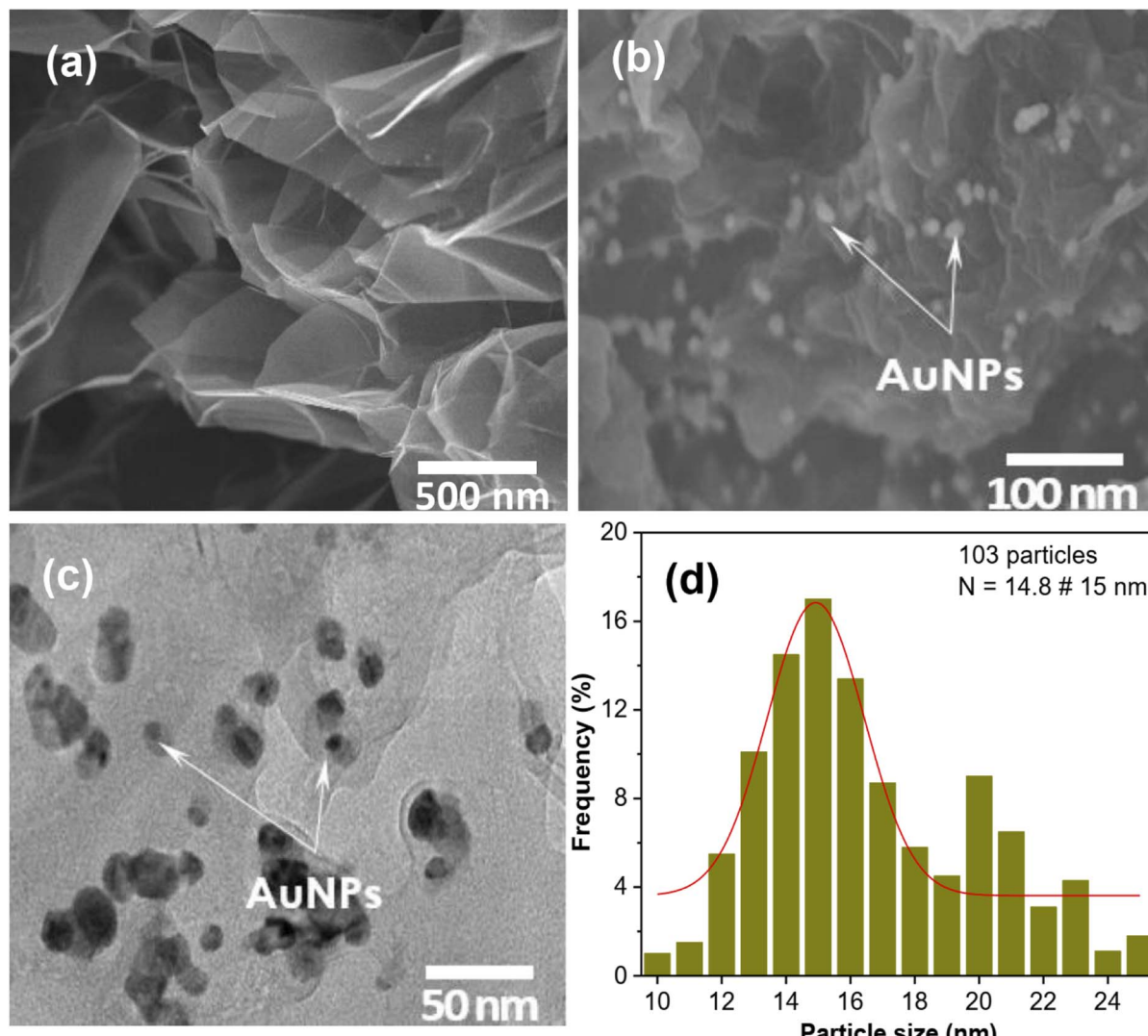


Fig. 2 SEM images of GO (a) and GO-AuNPs (b); TEM image of GO-AuNPs (c) and size distribution of AuNPs (d).

sputtering technique. In which, the finger-typed electrode deposited on the top of the structure is made of Ag with a thickness of 200 nm, and the rear electrode is made of Ti (50 nm)/Ag (200 nm). The hybrid solar cells with only PEDOT:PSS and PEDOT:PSS/GO are also prepared with the same conditions for comparison.

2.4. Characterization

The morphology of the samples was analyzed using SEM (Hitachi S4800) and HRTEM (Jeon-JEM 2100). A JASCO V-770 spectrophotometer was used to measure the absorption spectra. The XRD pattern was measured by using a XRD Bruker D8 Endeavor equipped with $\text{CuK}\alpha$ radiation. The Raman spectra of samples were recorded by using XploRA, Horiba Jobin-Yvon spectroscopy. The NPS Sigma-5+ based on 4-point technique were used to measure the sheet resistance of the PEDOT:PSS/GO-AuNPs thin film. The PCE of the hybrid solar

cells was measured with a Keithley 2400 source meter under AM 1.5 G with 100 mW cm^{-2} illumination.

3. Results and discussions

Fig. 2a shows the FESEM image of GO with an average thickness estimated to be few nanometers prepared by using the Hummers' method. Fig. 2b shows the FESEM images of GO-AuNPs hybrid materials, in which GO with AuNPs attached by chemical reduction method. Fig. 2c is a TEM image of the hybrid material sample. From the TEM image, as can be seen that AuNPs are tightly attached to the graphene sheets. Statistical analysis showed that the average size of AuNPs in the hybrid material was about 15 nm (Fig. 2d). Most of the particles were of medium size, but a few particles $> 20 \text{ nm}$ were also found in the sample. The average size distribution of AuNPs depends on the solvent medium and also on the GO content in the solution. This issue will be studied in the following sections.

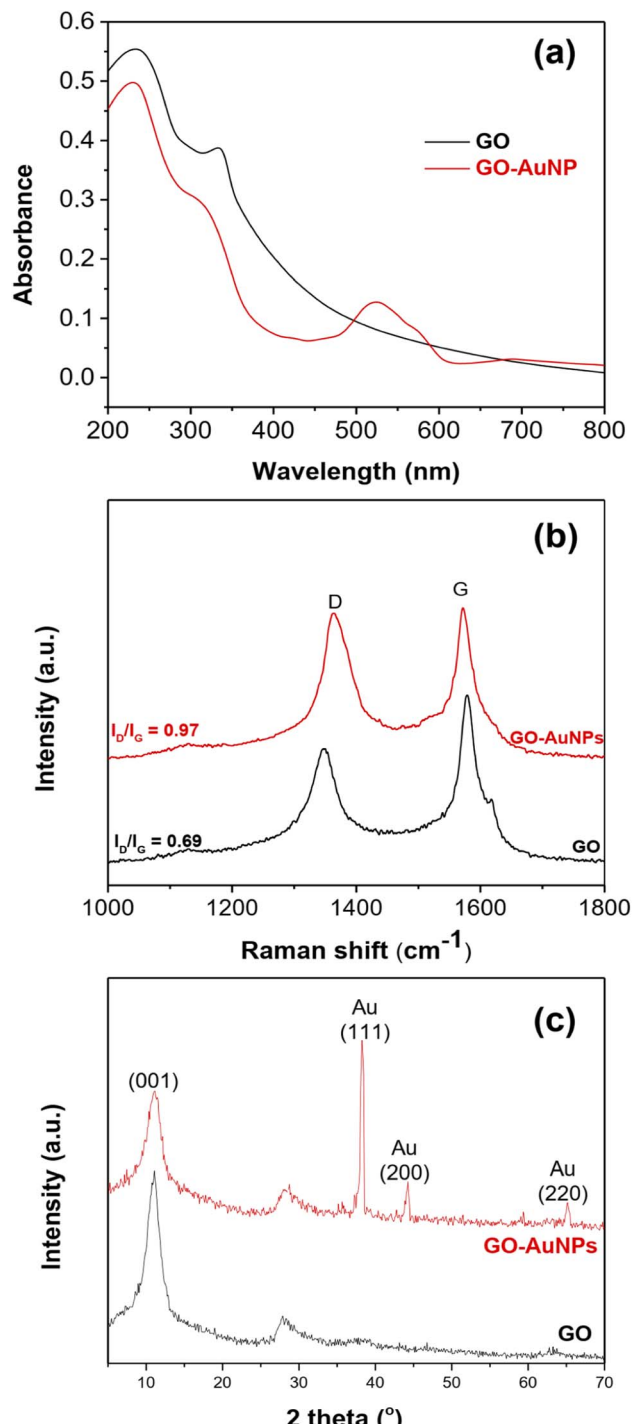


Fig. 3 (a) Optical absorption spectra, (b) Raman spectra and (c) XRD pattern of GO and GO-AuNPs.

UV-vis spectroscopy was used to validate the formation of GO-AuNPs hybrid material. The UV-vis spectra of GO and GO-AuNPs is presented in Fig. 3a. The UV-vis spectra of GO exhibit two peaks at 249 and 344 nm. This is attributed to the $\pi \rightarrow \pi^*$ aromatic C-C and C=C phase transition.⁴⁰ Two peaks with a red shift can be seen in the UV-vis spectra of GO-AuNPs. These peaks are attributable to the aromatic C-C transition of

GO and the surface plasmon resonance of AuNPs, respectively.^{41,42} These results provide more evidence that GO-AuNPs hybrid materials were formed. Fig. 3b shows Raman scattering confirming the transition between GO and GO-AuNPs. Raman spectra of GO exhibits D and G peaks at 1350 cm⁻¹ and 1579 cm⁻¹, respectively. The intensity ratio between D and G peaks (I_D/I_G) of GO-AuNPs (1.05) is higher than that of GO (0.68), which indicates that the appearance of AuNPs on the surface of GO causes some lattice defects in terms of structure compared to the original. Fig. 3c shows the XRD pattern of GO, and GO-AuNPs. The XRD of GO shows a typical peak at $2\theta = 10.90^\circ$, indicated that the graphite has been completely separated into graphene sheets. XRD of the GO-AuNPs hybrid material shows some typical peaks at 38.20°, 44.30° and 65.20° corresponding to the (111), (200) and (220) planes, respectively which are assigned to the Au-centered cubic plane. The obtained results confirmed that Au(1) was completely converted to Au(0). The average diameter of AuNPs of about 15.2 nm was calculated using the Scherer equation. This result is reasonably accurate compared to the data obtained from SEM and TEM measurements. Thus, the XRD results demonstrated that AuNPs were successfully attached on the surface of GO sheets to form GO-AuNPs hybrid material.

The optical and electrical properties of the PEDOT:PSS/GO-AuNPs compound were investigated in order to determine the impact that the GO-AuNPs hybrid material had on these characteristics. Fig. 4a shows the SEM image of the PEDOT:PSS/GO-AuNPs conductive thin film on a glass substrate. As observed, the thickness of the film was measured about 50 nm. The transmittance of PEDOT:PSS/GO-AuNPs film is shown in Fig. 4b. It can be found that when compared with thin films containing only GO, the transmittance of films containing GO-AuNPs is lower. The transmittance at 550 nm was determined to be 86.6%, 71.6% and 69.7% for the PEDOT:PSS, PEDOT:PSS/GO and PEDOT:PSS/GO-AuNPs thin films, respectively. Surface resistance of the PEDOT:PSS, PEDOT:PSS/GO and PEDOT:PSS/GO-AuNPs thin films are shown in Fig. 4c. The sheet resistance values were measured to be 249.6, 150.7 and 50.5 $\Omega \Omega^{-1}$ corresponding to PEDOT:PSS, PEDOT:PSS/GO and PEDOT:PSS/GO-AuNPs thin film, respectively. As a result, the incorporation of the GO resulted in a reduction in the sheet resistance of the PEDOT:PSS thin film. Notably, when using the hybrid GO-AuNPs material, the surface resistance is significantly reduced. The decrease in the sheet resistance for thin films containing GO-AuNPs hybrid materials was attributed to be the presence of good conductive AuNPs attached to the functional group sites on the surface of the graphene sheets.

I-V characteristic measurement is used to accurately evaluate the electrical properties of thin films. The thin film is fabricated on a glass substrate and all electrode connections are made with the help of gold wire. Gold wires are mounted on thin film at four corners with silver glue. All connections are made out according to the Van der Pauw four-probe method.⁴³ The in-plane conductivity of the films was estimated using the following eqn (1):⁴⁴



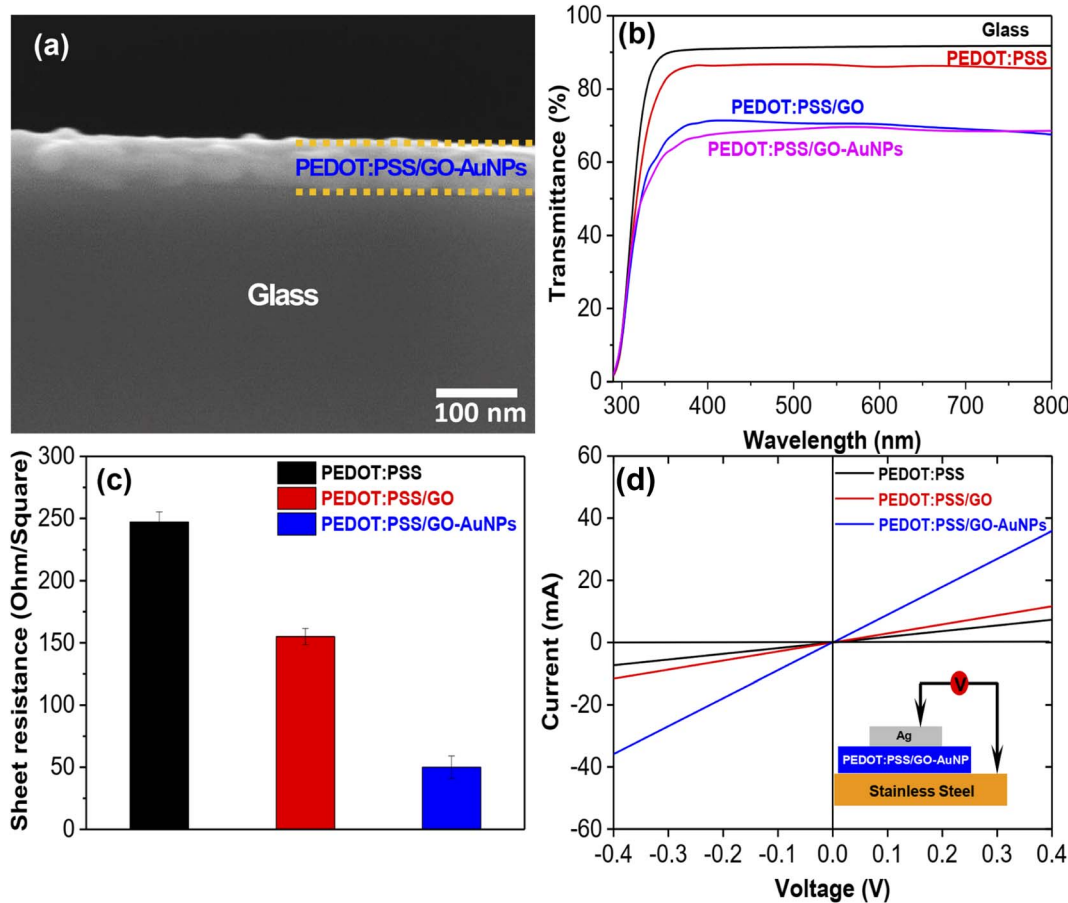


Fig. 4 (a) SEM image of conductive thin film PEDOT:PSS/GO-AuNPs, (b) transmittance, (c) surface resistance and (d) current–voltage (*I*–*V*) characterization of PEDOT:PSS, PEDOT:PSS/GO and PEDOT:PSS/GO-AuNPs films.

$$\sigma = \frac{\ln 2}{\pi d} \left(\frac{I}{V} \right) \quad (1)$$

where σ is the conductivity of the film sample, d is the thickness of the TCF film, I is the current through the film and V is the voltage across the thin film. Fig. 4d shows the current–voltage (*I*–*V*) response of a PEDOT:PSS thin film containing GO and GO-AuNPs hybrid material. For the conductivity measurement, the values of the film thickness are obtained from the SEM analysis. By using the eqn (1), the conductivity values were calculated to be 807 S cm^{-1} , 1284 S cm^{-1} and 3960 S cm^{-1} corresponding to the PEDOT:PSS, PEDOT:PSS/GO and PEDOT:PSS/GO-AuNPs thin film, respectively. Meanwhile, the conductivity of PEDOT:PSS/GO-AuNPs thin film is about 3 times higher than that of the PEDOT:PSS and PEDOT:PSS/GO thin film. The enhancement in the conductivity could be observed on *I*–*V* characteristics. It is clearly indicated that for a particular voltage range, the current increases with the film containing GO-AuNPs hybrid materials. This is because of the electrostatic interaction that occurs between AuNPs and the PSS chains. The electrostatic screening effect helped to reduce the interaction between PEDOT and PSS, which in turn helped to improve the connection between the PEDOT chains. As a consequence, the

electrons were able to move freely within the PEDOT chains, which resulted in improved electrical conductivity.

Characteristics of n-Si/PEDOT:PSS/GO-AuNP hybrid solar cells, including energy diagram and current–voltage (*I*–*V*) curves, are shown in Fig. 5. In this configuration, n-type Si served as both the light-absorbing layer and the electron–hole pair generator. The PEDOT:PSS layer functions as a p-type semiconductor material as well as a hole transport layer. The separation of electron–hole pairs takes place at the Si/PEDOT:PSS interfaces (Fig. 5a). The properties of the n-Si/PEDOT:PSS hybrid solar cells with different compositions are shown in Fig. 5b and Table 1. From the *J*–*V* characteristics, the n-Si/PEDOT:PSS hybrid solar cells without GO, the achieved PCE is 5.81% with a short circuit current density (J_{SC}) of 25.01 mA.cm^{-2} , an open circuit voltage (V_{OC}) of 0.484 V and a fill factor (FF) of 48%. When the GO component is added, the efficiency of the devices increases to 7.58%. The hybrid solar cell containing GO-AuNPs showed the highest PCE of 8.39% with a J_{SC} of 26.23 mA.cm^{-2} V_{OC} of 0.525 V and an FF factor of 61%, which are higher than those of the solar cell with PEDOT:PSS only. The obtained results are consistent with previous reports.^{45–48} According to Lu *et al.*, the PCE of a SiNHs/PEDOT:PSS hybrid solar cell including AuNPs was 6.1%, which is a 27% improvement over the solar cells without

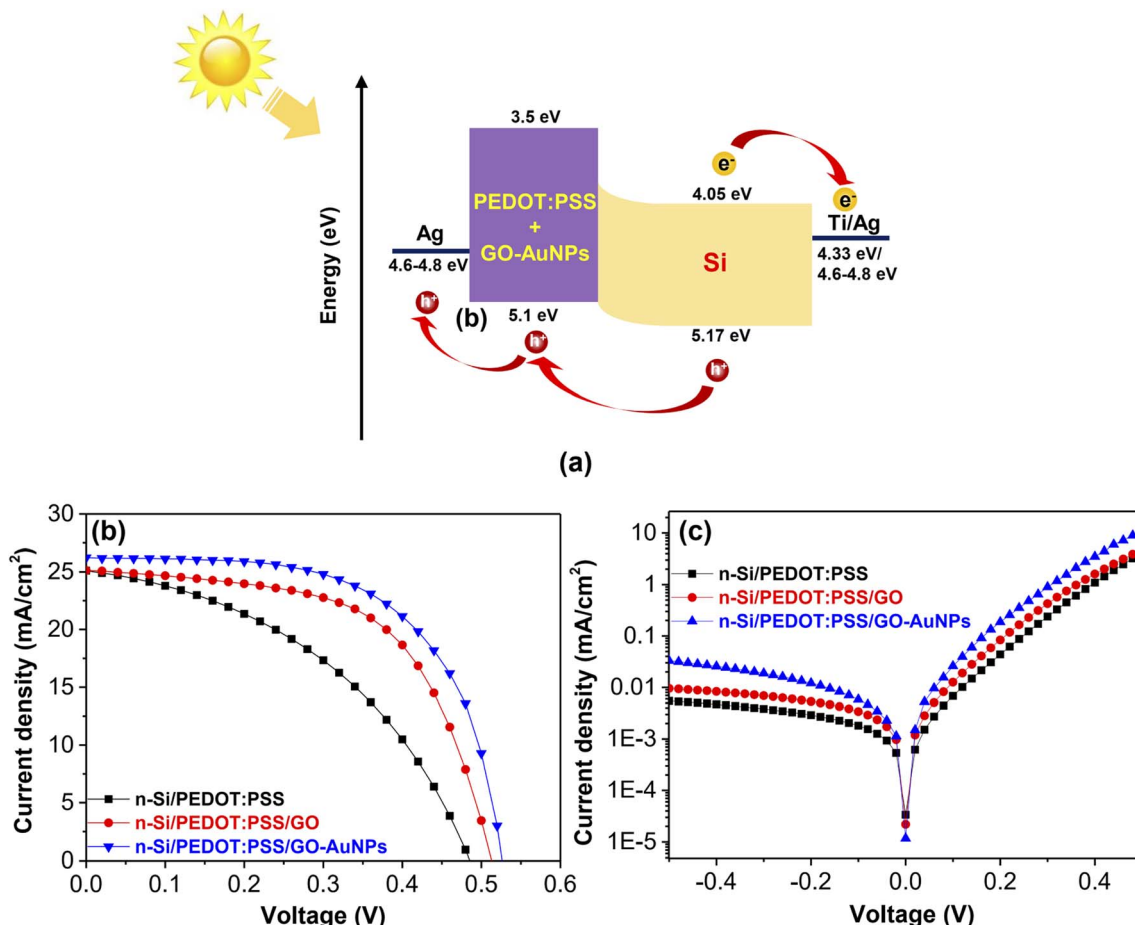


Fig. 5 (a) Energy diagram, (b) light illumination and (c) dark J–V characteristics of n-Si/PEDOT:PSS/GO-AuNPs hybrid solar cells.

Table 1 Characteristics of hybrid solar cells: short circuit current density (J_{SC}), open circuit voltage (V_{OC}), fill factor (FF), and power conversion efficiency (PCE)

Composition	J_{SC} (mA cm $^{-2}$)	V_{OC} (V)	FF (%)	PCE (%)
n-Si/PEDOT:PSS	25.01	0.484	48	5.81
n-Si/PEDOT:PSS/GO	25.12	0.512	58	7.58
n-Si/PEDOT:PSS/GO-AuNPs	26.23	0.525	61	8.39

AuNPs.⁴⁵ Similarly, Sharma *et al.* found an 8.2% PCE for planar Si/PEDOT:PSS/AuNPs, which is greater than the device without AuNPs (7.3%).^{46,47} Kim and colleagues reported a higher PCE for Si/PEDOT:PSS/AuNPs hybrid solar cells, with an *in situ* method measuring a PCE of 11.19% for the device containing AuNPs, roughly 19% higher than the device without AuNPs (9.42%).⁴⁸ Incorporating carbon nanomaterials into PEDOT:PSS allowed Uma *et al.* to achieve a PCE of 9.57% in hybrid solar cell containing GO. However, it is important to note that this structure required the use of silicon nanowires (SiNW) as substrate to improve the light absorption.⁴⁹ The increased PCE of solar cells with the addition of GO-AuNPs could be attributed to the increase of the conductivity of the PEDOT:PSS/GO-AuNPs compound. Besides, there is a possibility that the AuNPs

served as antennae for the incident light, leading to the improvement. Energy could be stored in a confined surface plasmon mode using these antennae.^{50,51} The trend of increasing and decreasing the conversion efficiency of solar cells is almost similar to the increase and decrease of conductivity of PEDOT:PSS/GO-AuNPs films. Furthermore, the presence of AuNPs in the hybrid solar cell will improve the optical absorption of the PEDOT:PSS/AuNPs resulted from the light-trapping effect of AuNPs at wavelengths below 500 nm. Consequently, the external quantum efficiency (EQE) of the hybrid solar cell will be enhanced in the wavelength range from 300 to 600 nm as addressed in the previous work.^{50,51} The dark J–V characteristic curve of the solar cell is shown in Fig. 5c. The obtained results show that GO-AuNPs hybrid materials have an effect on the properties of the hybrid solar cells. As a result, the devices that included GO-AuNPs exhibited the lowest current density. The obtained results exhibited that the decrease in the leakage current is much improved in comparison to the solar cell containing GO or pristine PEDOT:PSS. The device that has a smaller leakage current will hold higher values of V_{OC} , which will result in an increase in the efficiency.^{50,51} Thus, the PEDOT:PSS/GO-AuNPs compound is a promising materials for hybrid solar cells to achieve high PCEs.



4. Conclusions

Chemical reduction was used to prepared gold nanoparticles decorated graphene oxide hybrid material. The results reveal that 15 nm-diameter AuNPs are well decorated on the surface of GO. The hybrid materials were used to fabricate the TCF and the hybrid solar cell. The obtained results revealed that the TCF containing 0.5 wt% GO-AuNPs hybrid material has a transmittance of 69.7% at 550 nm, a low plate resistance of $50.5 \Omega \square^{-1}$. The hybrid solar cell incorporating GO-AuNPs had a PCE reached up to 8.39%, which is higher compared to the solar cell containing pristine PEDOT:PSS and PEDOT:PSS/GO. These findings demonstrated that the GO-AuNPs hybrid material is a promising material for enhancing the performance of the optoelectronics devices.

Conflicts of interest

There are no conflicts to declare.

Acknowledgements

This research is funded by Institute of Materials Science, Vietnam Academy of Science and Technology under project CS.11/21-22.

References

- S. K. Krishnan, E. Singh, P. Singh, M. Meyyappan and H. S. Nalwa, *RSC Adv.*, 2019, **9**, 8778–8881.
- W. Yu, L. Sisi, Y. Haiyan and L. Jie, *RSC Adv.*, 2020, **10**, 15328–15345.
- K. N. AK Geim, *Nature*, 2007, **6**, 183–191.
- J. K. Saha and A. Dutta, *Waste Biomass Valorization*, 2022, **13**, 1385–1429.
- N. N. Anh, N. v. Chuc, B. H. Thang, D. D. Phuong, P. v Trinh, P. N. Minh, N. Ngoc Anh, N. van Chuc, B. Hung Thang, P. van Nhat, N. Hao, D. Dinh Phuong, P. Ngoc Minh, T. Subramani, N. Fukata, P. van Trinh, P. v Nhat, N. v Hao, T. Thinh Ward, T. Nguyen, V. T. Subramani and N. Fukata, *Global Challenges*, 2020, **4**, 2000010.
- N. A. Nguyen, V. H. Nguyen, V. N. Pham, T. T. Le, V. T. Nguyen and V. T. Pham, *Adv. Nat. Sci.: Nanosci. Nanotechnol.*, 2021, **12**, 035009.
- P. N. D. Duoc, N. H. Binh, T. van Hau, C. T. Thanh, P. van Trinh, N. V. Tuyen, N. van Quynh, N. van Tu, V. Duc Chinh, V. Thi Thu, P. D. Thang, P. N. Minh and N. van Chuc, *J. Hazard. Mater.*, 2020, **400**, 123185.
- N. van Hao, N. van Dang, D. H. Tung, P. T. Tan, N. van Tu and P. van Trinh, *RSC Adv.*, 2020, **10**, 41237–41247.
- F. Schwierz, *Nat. Nanotechnol.*, 2010, **5**(7), 487–496.
- M. S. Jang, H. Kim, Y. W. Son, H. A. Atwater and W. A. Goddard, *Proc. Natl. Acad. Sci. U. S. A.*, 2013, **110**, 8786–8789.
- M. A. Giambra, A. Benfante, R. Pernice, V. Miseikis, F. Fabbri, C. Reitz, W. H. P. Pernice, R. Krupke, E. Calandra, S. Stivala, A. C. Busacca and R. Danneau, *ACS Omega*, 2019, **4**, 2256–2260.
- X. Han, H. Kong, T. Chen, J. Gao, Y. Zhao, Y. Sang and G. Hu, *Nanomaterials*, 2021, **11**, 2158.
- Z. Zhang, H. Huang, X. Yang and L. Zang, *J. Phys. Chem. Lett.*, 2011, **2**, 2897–2905.
- F. Ricciardella, S. Vollebregt, T. Polichetti, M. Miscuglio, B. Alfano, M. L. Miglietta, E. Massera, G. di Francia and P. M. Sarro, *Nanoscale*, 2017, **9**, 6085–6093.
- A. Zandiatashbar, G. H. Lee, S. J. An, S. Lee, N. Mathew, M. Terrones, T. Hayashi, C. R. Picu, J. Hone and N. Koratkar, *Nat. Commun.*, 2014, **5**, 1–9.
- L. Vicarelli, S. J. Heerema, C. Dekker and H. W. Zandbergen, *ACS Nano*, 2015, **9**, 3428–3435.
- L. Liu, M. Qing, Y. Wang and S. Chen, *J. Mater. Sci. Technol.*, 2015, **31**, 599–606.
- G. H. Moon, Y. Park, W. Kim and W. Choi, *Carbon*, 2011, **49**, 3454–3462.
- S. Gupta, A. Banaszak, T. Smith and N. Dimakis, *J. Raman Spectrosc.*, 2018, **49**, 438–451.
- R. K. Soraki, M. Gerami and M. Ramezani, *BMC Plant Biol.*, 2021, **21**, 1–14.
- A. Jana, E. Scheer and S. Polarz, *Beilstein J. Nanotechnol.*, 2017, **8**, 688–714.
- L. L. Shiau, S. C. K. Goh, X. Wang, M. Zhu, C. S. Tan, Z. Liu and B. K. Tay, *IEEE Trans. Nanotechnol.*, 2019, **18**, 1114–1118.
- C.-H. Shin, G. Park, C. Zhang and J.-S. Yu, *ECS Meeting Abstracts*, 2021, **01**, 470.
- A. Gutés, B. Hsia, A. Sussman, W. Mickelson, A. Zettl, C. Carraro and R. Maboudian, *Nanoscale*, 2012, **4**, 438–440.
- F. Parnianchi, M. Nazari, J. Maleki and M. Mohebi, *Int. Nano Lett.*, 2018, **8**(4), 229–239.
- C. Xu, X. Wang and J. Zhu, *J. Phys. Chem. C*, 2008, **112**, 19841–19845.
- C. Wang and D. Astruc, *Prog. Mater. Sci.*, 2018, **94**, 306–383.
- Y. J. Zhang, M. K. Geng, H. Zhang, Y. He, C. Peng, Q. Huang and C. H. Fan, *Chin. Sci. Bull.*, 2012, **57**(23), 3086–3092.
- D. Shin, H. R. Kim and B. H. Hong, *Nanoscale Adv.*, 2021, **3**, 1404–1412.
- D. O. Idisi, E. M. Benecha, S. J. Moloi and S. C. Ray, *J. Mater. Res.*, 2022, **37**(5), 1037–1046.
- Y. Si and E. T. Samulski, *Chem. Mater.*, 2008, **20**, 6792–6797.
- H. W. Tien, Y. L. Huang, S. Y. Yang, J. Y. Wang and C. C. M. Ma, *Carbon*, 2011, **49**, 1550–1560.
- C. Jin, J. Wang, S. Zhang, F. Liu, K. Liao and M. Han, *Nanotechnology*, 2019, **30**, 495203.
- Y. Liu, F. Wang, L. Li, F. Cao, B. Zhu, B. Zhu, Y. Gu and Y. Gu, *J. Opt. Soc. Am. B*, 2022, **39**(3), 713–721.
- J. Wu, Y. Xu, P. Xu, Z. Pan, S. Chen, Q. Shen, L. Zhan, Y. Zhang and W. Ni, *Nanoscale*, 2015, **7**, 17529–17537.
- M. Cittadini, M. Bersani, F. Perrozzi, L. Ottaviano, W. Włodarski and A. Martucci, *Carbon*, 2014, **69**, 452–459.
- M. K. Chuang, S. W. Lin, F. C. Chen, C. W. Chu and C. S. Hsu, *Nanoscale*, 2014, **6**, 1573–1579.
- Z. Zhao and Q. Wang, *Instrumentation Sci. Tech.*, 2022, **50**(5), 530–542.



39 N. F. Chiu, C. C. Chen, C. du Yang, Y. S. Kao and W. R. Wu, *Nanoscale Res. Lett.*, 2018, **13**, 1–11.

40 H. Wang, J. Chen, C. Duan, X. Xu, Y. Zheng, J. U. Grabow, Q. Gou and W. Caminati, *J. Phys. Chem. Lett.*, 2021, **12**, 5150–5155.

41 J. Huang, L. Zhang, B. Chen, N. Ji, F. Chen, Y. Zhang and Z. Zhang, *Nanoscale*, 2010, **2**, 2733–2738.

42 D. Hernández-Sánchez, G. Villabona-Leal, I. Saucedo-Orozco, V. Bracamonte, E. Pérez, C. Bittencourt and M. Quintana, *Phys. Chem. Chem. Phys.*, 2018, **20**, 1685–1692.

43 F. S. Oliveira, R. B. Cipriano, F. T. da Silva, E. C. Romão and C. A. M. dos Santos, *Sci. Rep.*, 2020, **10**, 1–8.

44 A. C. Bhowal, H. Talukdar and S. Kundu, *Polym. Bull.*, 2018, **76**(10), 5233–5251.

45 R. Lu, L. Xu, Z. Ge, R. Li, J. Xu, L. Yu and K. Chen, *Nanoscale Res. Lett.*, 2016, **11**, 1–7.

46 M. Sharma, P. R. Pudasaini, F. Ruiz-Zepeda, D. Elam and A. A. Ayon, *ACS Appl. Mater. Interfaces*, 2014, **6**, 4356–4363.

47 M. Sharma, R. Lopez-Delgado and A. A. Ayon, *Microsyst. Technol.*, 2017, **24**(1), 543–550.

48 W. H. Kim, S.-J. Sung, K.-P. Kim, D.-K. Hwang and S. Woo, *Sci. Adv. Mater.*, 2018, **10**, 560–564.

49 K. Uma, T. Subramani, H. J. Syu, T. C. Lin and C. F. Lin, *J. Appl. Phys.*, 2015, **117**, 105102.

50 P. van Trinh, N. N. Anh, N. T. Bac, C. T. Anh, N. van Hao, L. H. Chi, B. H. Thang, N. van Chuc, P. N. Minh and N. Fukata, *Mater. Sci. Semicond. Process.*, 2022, **137**, 106226.

51 P. van Trinh, N. N. Anh, N. T. Cham, L. T. Tu, N. van Hao, B. H. Thang, N. van Chuc, C. T. Thanh, P. N. Minh and N. Fukata, *RSC Adv.*, 2022, **12**, 10514–10521.

